A separated jet and coastal counterflow during upwelling relaxation off Cape São Vicente (Iberian Peninsula)

Paulo Relvas[1,*] and Eric D. Barton[2]

[1] **Centro de Investigação Marinha e Ambiental**

Universidade do Algarve - Campus de Gambelas

8000-117 Faro

PORTUGAL

E-mail: prelvas@ualg.pt

Fax: +351-289818560

[2] **School of Ocean Sciences**

University of Wales - Menai Bridge

Gwynedd - Wales LL59 5AB

UNITED KINGDOM

E-mail: e.d.barton@bangor.ac.uk

* Corresponding author

A separated jet and coastal counterflow during upwelling relaxation off Cape São Vicente (Iberian Peninsula)

ABSTRACT – The circulation and structure of the coastal upper ocean during the relaxation after an upwelling event around Cape São Vicente, the southwestern tip of Iberian Peninsula, are described. Hydrographic, ADCP, wind, and remotely sensed SST data during the upwelling season reflect the interplay of two contrasting regimes in the region: coastal upwelling and a nearshore countercurrent. The observations revealed a 40 km wide jet-like flow, separated from the coast, that advected cold water southward off the west coast and eastward around the Cape. It originated prior to the cruise in the upwelling that occurred off prominent west coast capes north of the sampling region. Adjacent to the coast, a narrow inshore counterflow advected warm water westward along the south coast, curled anticyclonically around the Cape with velocities up to $0.4\,\mathrm{ms}^{-1}$, and progressed poleward inshore of the previously upwelled water. The cold equatorward jet interacted with offshore waters and inshore countercurrent by generating small scale instabilities, and weakened as it proceeded south and around the Cape. The inshore countercurrent was suppressed during the final part of the survey by an eastward flow associated with a return to upwelling favourable wind off the south coast of Portugal.

Keywords: Coastal oceanography; Upwelling relaxation; Coastal countercurrents; Mesoscale features; Coastal upwelling; Eastern boundary currents; Iberian Peninsula, Portugal, Cape São Vicente.

1 Introduction

The coastal transition zone near Cape São Vicente (CSV) (9°W;37°N), where the meridional west and zonal south coasts of the Iberian Peninsula meet (Fig. 1), is markedly seasonal. During summer, the prevailing wind along the west coast blows from the north, as a consequence of the strengthening Açores high pressure cell in the central Atlantic and the weakening Iceland low. However, along the south coast, the summer wind is predominantly from the west. The establishment of a thermal low pressure centre over Iberia during summer diverts the near surface wind field eastward over southern Portugal. A zonal ridge along the Algarve, highest (≈900 m) in the west, may contribute to the deformation of the wind field. Under these winds the coastal region off western and southern Portugal exhibits the classical circulation of eastern boundary regions - wind-forced near-surface offshore transport, upwelling of cold subsurface waters at the coast and the generation of alongshore currents.

Satellite imagery and *in situ* observations of the coastal ocean reveal a surface poleward current as a persistent feature of the winter circulation off western Iberia. This structure appears as a warm and saline intrusion (temperature $1-3$°C and salinity 0.2-0.3 higher than surrounding values), within about 50 km of the shelf break, 200-600 m deep, and flowing along the slope at 0.2-0.3 ms^{-1}, with transport increasing downstream (Frouin et al., 1990; Haynes and Barton, 1990). Possible generation mechanisms include density and wind forcing. The geostrophic flow of the northeast Atlantic is eastward in a broad band north of 33°N, where a meridional density gradient, associated with the poleward cooling of the sea surface, is observed in the upper 200-300 meters (Pollard and Pu, 1985). Such a density gradient can force a poleward current, intensified over the slope and increasing northward (Huthnance, 1984). Intensification of the Iceland low pressure cell associated with a large southward displacement of the Açores high pressure cell results in a wind pattern with a southerly component, particularly in the northern part of the Iberian Peninsula. Such a wind pattern can contribute to the generation of the observed winter poleward current off Iberia (Frouin et al., 1990).

During the March-September upwelling season, northerly winds, strongest in July-August (Wooster et al., 1976; Fiúza et al., 1982), drive an offshore Ekman transport and force subsurface waters to upwell along the coast. Upwelling responds quickly to northerly winds, particularly south of capes, appearing first along the coastline and then spreading offshore as the event progresses (Fiúza et al., 1982). During the upwelling period, the wind forcing opposes the density forcing. Upwelling causes the surface dynamic height to decrease towards the coast and the resulting equatorward geostrophic current can counter the poleward slope current at and near the surface, establishing a southward flow. However, waters below 100-200 m still flow poleward as an undercurrent (Haynes and Barton, 1990). On occasion, water upwelled on the west coast extends around CSV eastward along the Algarve shelf (Fiúza, 1983). The south coast of Portugal is also directly affected by upwelling events under favourable westerly winds. These are usually weaker and more intermittent than on the west coast and occur mainly during late spring/summer (Relvas and Barton, 2002). The intensity and frequency of the upwelling decreases from west to east along the south coast (Fiúza, 1983). During the upwelling season therefore, coastal flow off southern Algarve is generally eastward, as a result of west coast upwelling or of locally induced upwelling.

The undercurrent advects predominantly subtropical and Mediterranean waters northward. Below the surface layer the waters are typically a subdivision of North Atlantic Central Water termed Eastern North Atlantic Central Water with subtropical origin (Fiúza, 1982). In winter this water reaches the surface and extends down to the warm and saline Mediterranean Water (MW). The shallowest MW lies at 400 m or less off southwestern Iberia (Ambar, 1983) as the continuation of a vein flowing along the shelf break in the Gulf of Cadiz (Meincke et al., 1975; Zenk, 1975; Ambar and Howe, 1979). The main core of MW occupies deeper layers down to 1500 m. Most of the previous research in the area was related to the Mediterranean outflow and associated features, which occur at deeper levels (Meincke et al., 1975; Zenk and Armi, 1990; Rhein and Hinrichsen, 1993), and the structure of the upper ocean in the region is poorly understood.

Figure 1: Transects during the Poseidon 201/9 survey (**a**), the Cape São Vicente region (**b**) and general bathymetry and orography (**c**). Arrows denote the steaming direction and dots the CTD stations. Bathymetric contours are in meters.

This paper addresses the detailed circulation and structure in the upper layers off the southwest tip of Iberia Peninsula (Fig. 1) during a short period of the summer upwelling season. Because of the 90° bend in the coast at Cape São Vicente (CSV), the situation is more complex than in areas of simple topography, where most upwelling studies have taken place. Satellite imagery shows that a recurrent filament of cold, upwelled water extends offshore from CSV during periods of persistent northerly winds, while the rapid development of a warm coastal counter-current accompanies relaxation of upwelling-favourable winds. The near-shore counterflow extends from the Gulf of Cádiz, around CSV and northward as far as 38°N. This narrow (15-25 km), warm current separates the cold upwelled water from the coast and the filament from its origin at CSV if it is present (Relvas and Barton, 2002). The aims of the study were to observe the sub-surface structure and document the space and time scales of these features, previously observed only in remote sensing.

In this paper we document the onset of the inshore countercurrent and its interaction with a cold, southward upwelling jet that separates from capes further north at 39°N. We present direct observations of the structure of the warm inshore countercurrent and associated circulation around CSV in relation to the mesoscale features seen in satellite sea surface temperature imagery. The study reveals the importance of relaxation events during the upwelling season, in rapidly introducing distinct waters into the coastal zone, with important implications for spread of contaminants and harmful algal blooms.

2 Sampling and data processing

Hydrography

Sampling was carried out initially along four zonal transects and two meridional transects at half degree intervals (about 55 km in latitude and 45 km in longitude) around

CSV (Fig. 1**a**). Subsequent sampling was guided by Advanced Very High Resolution Radiometer (AVHRR) satellite images, processed and transmitted to the ship in near real time. It comprised 10×10 km grids off the west and south coasts and a transect southwest from CSV. A total of 132 CTD stations were sampled with a self-contained Sea-Bird Electronics 19 Seacat Profiler. Station separation was generally 10 km, but 5 km in two nearshore transects. Casts were made to 500 meters depth or to 5 meters above the bottom in shallower water. The sampling rate was 2 scans per second and the lowering speed was $1\,\mathrm{ms}^{-1}$ Data were processed by excluding erroneous scans, applying conductivity and temperature corrections determined from *in situ* calibration samples, and averaging the calculated salinity and temperature data into 2 dbar bins. Details of the survey, processing stages, and the complete CTD data set are presented by Relvas and Barton (1995). The calibrated data were used to derive density and dynamic height anomaly with standard algorithms (UNESCO, 1991).

Dynamic height of the sea surface ($p = p_{sup}$) was calculated with respect to the 500 dbar reference level ($p = p_{ref}$) and was normalized by the acceleration of gravity ($\Delta D_{p_{sup}/p_{ref}}/g$). The calculation was extended to shallower stations by the linear extrapolation method of Reid and Mantyla (1976). The dynamic height contours would represent geostrophic streamlines if the velocity at the reference level were everywhere zero. The chosen reference level is deep enough to suppose a level of no or weak motion, yet shallow enough to avoid the influence of the main cores of the Mediterranean outflow. A similar pressure level has proved to be an acceptable reference level in the California upwelling system (e.g., Ramp et al., 1991). However, strong motion at the Mediterranean Water depths might influence the surface topography, in particular during the occurrence of meddy features (Oliveira et al., 2000). The shallow vein of Mediterranean water seen as a narrow feature near 500 dbar in the present observations does not significantly distort the dynamic height field.

Acoustic Doppler profiler velocity

Upper-ocean currents were measured along the ship's track with a hull-mounted RDI narrow band acoustic Doppler current profiler (ADCP) operating at 150 kHz. Details of the ADCP data processing and a presentation of the complete data set are reported by Relvas and Barton (1996). The ADCP transducer transmitted pulses with 16 m length in four independent beams oriented at a 30° angle from the vertical axis of the ship. Approximately 100% of the pulses were returned above 250 m depth. The acceptance threshold for good data was set to 30%, corresponding to a depth of 475 m. The shallowest reliable data were from 16 m below the surface. Average profiles of water velocity relative to the ship were obtained once every 5 minutes with a vertical bin size of 8 m. Data processing was carried out using the common oceanographic data access system (CODAS) (Firing and Ranada, 1995). Most of the cruise was in deep water and so little bottom track data was collected. Following quality assessment of the ship's global positioning system (GPS) navigation data, a water-track calibration was applied (Pollard and Read, 1989) to compute the absolute currents referred to geographical coordinates.

ADCP data were averaged over selected distances along track and over set intervals in depth. The shallowest depth interval was taken as 16 to 25 m, and deeper ones were every 50 m. Current vector maps corresponding to consecutive subsets of the cruise track were built. Maps of the horizontal velocity field were built on data averaged over 0.05° in distance (5.56 km in longitude $\times$ 4.44 km in latitude) , while the detailed maps off the west and south coasts used averages over intervals with half of the size.

The lack of time series stations precluded accurate evaluation of the degree of contamination of the ADCP data by tidal currents. However, subsets of the data in restricted areas were treated as time series. Harmonic analyses of these subsets provided amplitude estimates for the main tidal constituents. A tidal model for six major constituents (M2, S2, K2, O1, P1 and Q1) run specifically for the CSV region showed maximal tidal currents of $0.07\,\mathrm{ms}^{-1}$ in a small near-shore region south of the Cape and less than $0.04\,\mathrm{ms}^{-1}$ elsewhere. Also, analysis of TOPEX/POSEIDON data (Fanjul et al., 1997) indicated M2 tidal currents of $0.05\,\mathrm{ms}^{-1}$ near 40°N, in agreement with the harmonic analyses. The

Figure 2: Wind stress time series at the coastal stations of Cabo Carvoeiro (**top** — for location see Fig. 4) and Sagres (**bottom**) from 20 May to 22 June 1994, computed from the original 6-hourly data.

typical velocity signal measured by the shipboard ADCP was much greater, therefore the tidal signal had negligible contribution to the observed velocity field. Moreover, subsequent analysis showed that the main features observed in the ADCP data were closely related with the observed hydrographic features. For these reasons, no correction of the ADCP data was attempted. Similarly, studies in the coastal transition zone off California have generally considered the effect of tidal currents on ADCP data to be negligible (e.g. Huyer and Kosro, 1987; Ramp et al., 1991; Huyer et al., 1991), and when it was evaluated the authors concluded that the effect was small (Barth and Brink, 1987).

Wind

Wind stress was computed from 6-hour wind data records at Cape Carvoeiro, on the west coast at 39.4°N, and Sagres, on the CSV cliffs (Fig. 2), using $\sigma_s = \rho_a C_s |\vec{V_a}| u_a$, where ρ_a represents the air density, $\vec{V_a} = (u_a, v_a)$ the wind vector, and C_s a non-linear wind stress drag coefficient based on Large and Pond (1981) modified for low wind speeds as in Trenberth et al. (1990) ($Cs = 0.00218$ for $|\vec{V_a}| \leq 1\,ms^{-1}$; $Cs = (0.62 + 1.56|\vec{V_a}|^{-1})\,0.001$ for $1\,ms^{-1} < |\vec{V_a}| < 3\,ms^{-1}$; $Cs = 0.00114$ for $3\,ms^{-1} \leq |\vec{V_a}| < 10\,ms^{-1}$; $Cs = (0.49 + 0.065|\vec{V_a}|)\,0.001$ for $|\vec{V_a}| \geq 10\,ms^{-1}$).

Wind stress computed from shipboard winds measured every four minutes and low pass filtered to remove oscillations of period less than six hours shows weak southward wind during a long period at the beginning of the campaign (Fig. 3). On 19 June, winds were northeasterly, then rotated anticlockwise to westerly, upwelling favourable off the south coast, for about 17 hours. They later rotated more to become variable from the north quadrant, upwelling favourable off the west coast. The last part of the cruise was carried out under strong northeasterly wind stress.

The winds measured at the nearby coastal meteorological station of Sagres (Fig. 2), on the CSV cliffs, were considerably different from the ship winds. Because only one of

Figure 3: Vector time series of the ship wind stress, presented unrotated (**top**), parallel to the west coast, and rotated clockwise by 90° (**bottom**), parallel to the south coast. Observations every 4 minutes were low pass filtered to remove oscillations with periods less than six hours. The timing of relevant transects are shown.

the two ship's anemometers was functioning properly, interference of the wind flow by the superstructure may have rendered the ship wind less reliable than normal. However, spatial inhomogeneity of the wind field around the area of CSV is probably the major factor for the differences between ship and shore winds. The latter confirm the weakness of the wind and the occurrence of northerly winds during 19-21 June.

Sea surface temperature

Sea surface temperature satellite images derived from NOAA-AVHRR sensors, providing a ground resolution of 1.1 km × 1.1 km at nadir, were used in the analysis. To all AVHRR images used in this paper, an atmospheric correction was applied by combining the brightness temperatures for channels 4 and 5 using the split window algorithm of McClain et al. (1985).

3 Results

3.1 The equatorward flow and the coastal countercurrent

The survey took place a few days after the cessation of upwelling events around 5 June off the west coast and around CSV (Fig. 2). The continuing favourable, though weak, wind between 8 and 12 of June at Cape Carvoeiro was not seen further south at Sagres. The remotely sensed sea surface temperature reflected this situation (Fig. 4). During the cruise (11 - 22 June) coastal winds were almost null, except in the last three days, when an upwelling event seen first at Sagres extended up the west coast to Cape Carvoeiro.

On 6 June, a band of cold upwelled water along the south and west coasts was interrupted only in the sheltered bights south of Lisboa and Cape Espichel, where higher sea surface temperatures signalled little upwelling (Fig. 4). The colder waters upwelled north of Cape Carvoeiro and Cape da Roca, separated from the shore at these capes

Figure 4: Sea surface temperature images of 6, 9 and 11 June 1994, showing the upwelling event off southwest Iberia and the development of a separated equatorward jet of cold upwelled water from further north, at the Cape Carvoeiro/Cape da Roca region.

to extend directly south. By 9 June, the separated tongue of upwelled water reached beyond Sines (38°N) along the shelf edge some 20 km offshore. Close to shore, upwelling persisted as far as CSV and, more weakly, along the Algarve coast. At the start of the cruise on 11 June, the separated cold tongue had weakened, but penetrated even further to about 37.5°N. Upwelling persisted north of and around Cape Carvoeiro with the continued weakly favourable wind stress there (Fig. 2), but had declined further south, where the wind was virtually null. To the east of CSV, warmer water had appeared along the Algarve coast inshore of cooler water over the shelf edge.

During the first survey (12-15 June) coastal upwelling was absent around CSV, and the AVHRR image of 16 June 1994 (Fig. 5**a**) indicated a post-upwelling pattern. A narrow band of warmer water, continuous from the Gulf of Cádiz, adjoined the coast to both sides of the cape. For reference, the $\Delta D_{0/500}$ contours and near surface ADCP current vectors for transects 1-5 west and southwest of CSV are overlaid on a subset of the image (Fig. 5**b**). The warm band lay generally inshore of the *in situ* sampling, but where they overlapped off CSV, northward surface velocities $>0.40\,\mathrm{ms}^{-1}$ along the temperature front suggested a coastal poleward counterflow. A broad band of cooler water along the west coast continental slope indicated the continuation of the cold tongue separating from Cape da Roca, while an even cooler strip of remnant locally upwelled water lay offshore and south of Cape Sines. The offshore boundary of the main cold tongue coincided with predominantly southward flow of up to $0.30\,\mathrm{ms}^{-1}$ along the strongest gradient of dynamic height. This cooler water turned eastward around the Cape to penetrate along the slope.

The ADCP velocities in the shear region with the coastal poleward counterflow west of CSV suggest that part of the southward flow turned cyclonically following the dynamic topography. Moreover, the current vectors suggest anti-cyclonic rotation on the offshore side of the cold tongue in transect 4 at 37.1°N, and cyclonic rotation in the center of tran-

Figure 5: AVHRR satellite sea surface temperature image of 16 June 1994 (**a**)off southern Iberia, and subsets of the same image (**b**) with the near surface (16-25 meters) ADCP current vectors for transect 1 to 5 and the $\Delta D_{0/500}$ field superimposed (**c**) for transect 6 to 8 and the $\Delta D_{0/30}$ field superimposed, and (**d**) the contour map of $\Delta D_{0/30}$ for the entire region. The scale of the ADCP vectors is shown in the panels. Station positions are denoted by dots along the ship track. Units of dynamic topography are $10\,\mathrm{m^2s^{-2}}$. Bathymetric contours are represented. Dark patches represent clouds.

sect 5 at 37.6°N. Also, some of the southward flow that turned CSV became incorporated into the coastal counterflow (Fig. 5**b**).

The maximum dynamic height in the area occurred in an anticyclonic eddy, centred at 36.6° N; 9.7° W. The ADCP currents on the transects through and south of the high indicate anticyclonic rotation with speeds up to 0.4 m/s about a centre slightly further west. The discrepancy in position may be caused by interpolation between the widely spaced transects and by ageostrophic components of the ADCP velocity. The anticyclonic circulation is possibly the surface signature of a deeper MW eddy (meddy), since these have been related to positive altimeter anomalies in the surface topography (Stammer et al., 1991; Hinrichsen et al., 1993; Tychensky and Carton, 1998) and are known to form off CSV (Prater and Sanford, 1994; Bower et al., 1997; Serra et al., 2002).

Before 19 June the survey experienced calm conditions, and so wind driven currents were negligible. The complex flow pattern was dominated by small scale instabilities. Given the 40-50 km spacing between transects, the dynamic topography could not resolve eddies or meanders with meridional scales of less than 80-100 km, except in the small grid (transects 6 to 8) close to CSV. There, features with alongshore scales of about 15-20 km could be resolved. Although the 3-day survey was completed one day before the image, so that temporal changes might have occurred, there was strong correspondence between features in the *in situ* and remotely sensed data.

Data from the fine-scale grid of 15-16 June superimposed on an enlargement of the satellite image of 16 June (Fig. 5**c**) indicate the warmer counterflow around the Cape turned anticyclonically against the west coast. ADCP velocities up to $0.40\,\mathrm{ms^{-1}}$ were consistent with the field of dynamic height ($\Delta D_{0/30}$), indicating strong near-surface shear.

The counterflow progressed northward, inshore of the remnant cool water from the earlier Cape Sines upwelling. Further offshore, northward velocities were weaker ($< 0.25\,\mathrm{ms}^{-1}$) and turned slightly westward to advect some of the warmer water offshore.

The $\Delta D_{0/30}$ field for the entire cruise (Fig. 5**d**) showed a tongue of low dynamic height along the southern continental slope close to CSV, coincident with the cold protrusion in sea surface temperature, with higher dynamic height near shore. This pattern again suggests a narrow surface coastal counter-current flowing westward along the coast of Algarve, turning northward around the Cape. The cyclonic eddy off the west coast was still evident in the$\Delta D_{0/30}$ map but the anticyclone around 36.6° N; 9.7° W (Fig. 5**b**) was almost undetectable. This indicates that the cyclonic, but not the anticyclonic, eddy was surface intensified, supporting the idea that the latter is a deeper meddy feature.

The near-surface ADCP velocity field of the south coast fine grid (transects 9 to 11 on 17-18 June) was superimposed on the AVHRR infrared image of 18 June 1994 (Fig. 6**a**). The cold water intrusion, which possibly included cold water upwelled locally before the cruise (as on 6 June), showed a wave-like perturbation in its offshore front with warmer oceanic waters. The current vectors showed a cyclonic tendency in the wave trough at 8.6° W but the flow pattern further inshore was undefined. A similar cyclonic pattern of the ADCP vectors, but not of dynamic heights, had been observed in this location during the initial stages of the cruise (Fig. 5**b**). The ADCP current and dynamic height fields were probably inconsistent because factors other than the Coriolis force and the horizontal pressure gradient influence these smaller scale instabilities. Moreover the assumption of 500 dbar as a level of no motion may be incorrect here because of the presence of the shallow vein of MW. The inshore water, warmer by >1.5°C, extended westward along the south coast and northward along the west coast. At deeper levels (Fig. 6 **b,c,d**) a small scale cyclonic eddy became evident, while in the deepest layer with reliable data (425-475 m) westward flow up to $0.30\,\mathrm{ms}^{-1}$ was found in the uppermost levels of MW (Fig. 6**e**) as reported by Ambar (1983).

Figure 6: ADCP current vectors for transect 9 to 11 (Jun 17 11:00 - Jun 18 17:00), for the (**a**) 16-25, (**b**) 25-75, (**c**) 75-125, (**d**) 275-325, and (**e**) 425-475 meters depth bins. The upper (16-25 m) ADCP vectors are superimposed on an enlarged view of the AVHRR satellite sea surface temperature of 18 June 1994, near CSV. The scale of the ADCP vectors is shown in the top panel. Bathymetric contours are represented.

Figure 7: AVHRR satellite sea surface temperature image of 20 June 1994, with the near surface layer (16-25 meters) ADCP current vectors for transect 12 to 13 (19 June 09:30 - 21 June 19:00) superimposed (**a**). Maps of the ADCP current vectors, for the (**b**) 25-75, (**c**) 75-125, and (**d**) 175-225 meters depth bins are shown. The scale of the ADCP vectors is shown in the top panel. Bathymetric contours are represented.

Forced by a pulse of favourable (up to 13.5 ms^{-1}) winds (Fig. 8**a**), an upwelling event was underway off the south coast when transects 12-13 were sampled between 19 and 21 June (Fig. 7**a**). The changing direction of the strong wind stress produced a marked response in the upper layer currents, which were quite different during the outward and return tracks along the 8.3°W transect 13. If the data out and back are treated as though obtained at a single point, the current vector is seen to rotate anticyclonically with close to the inertial period of 20.2 hour at 36.5°N (Figure 8**b**), and a good least squares fit of the inertial cycle can be made to the de-meaned observations. The progressive vector diagram comparing the original data with the least squares fit plus mean current (Figure 8**c**) shows the anticyclonic rotation superimposed on a southeastward drift. This is the inertial response of the upper ocean to the wind pulse just before the sampling of this line (Fig. 8**a**). Apart from this transient, the layer above 25 m showed an overall eastward advection of cold upwelled water over the continental shelf and slope, consistent with geostrophic adjustment via Ekman transport. The 25-75 m layer showed weak westward flow near shore, related to the coastal counterflow preceding the event. The counterflow was absent at shallower levels because it was masked by the wind stress acting above the thermocline depth of 30-40 m.

Surface fields for the entire cruise computed from the *in situ* measurements confirm the major features revealed in the satellite imagery (Fig. 9 **a, b, c**). Original data were not truly synoptic because of the time span of the survey and changes in the wind forcing.

Figure 8: Vector plots of the pseudo-time series of **(a)** shipboard wind measurements (19 Jun 20:25 to 21 Jun 09:32) and **(b)** ADCP velocities (16 - 25 m layer) for transect 13 and return track (20 Jun 12:14 to 21 Jun 09:32), related with the inertial event. **(c)** represents the simulated trajectory of a control particle as a progressive vector diagram. Dashed lines represent the least square fit of an inertial oscillation for 36.5°N and the labels represent the decimal days.

Figure 9: Horizontal fields of (**a**) temperature, (**b**) salinity and (**c**) density (σ_t) at 5 m depth observed during the Poseidon 201/9 survey. CTD stations are denoted by dots. Bathymetry is shown. (**d**) Mean summer (June to August) surface salinity around CSV, from the National Oceanographic Data Center database.

However, because wind strengthened only in the last days of the cruise, surface temperature patterns agree quite closely with those in the SST image of 16 June. Temperature and salinity fields do not show a simple meridional trend, because isolines parallel the south coast, round CSV and then turn northwest at an angle to the west coast bathymetry. To the south and southwest, all fields, including density, were quite homogeneous. Strongest surface gradients were restricted to the continental slope and shelf off the south coast, around CSV, and along a front to the northwest.

A conspicuous salinity front, over 0.5 in contrast, separated lower salinity shelf and slope waters from higher salinity offshore waters. This is part of the summer climatologic salinity front that occurs off southwest Iberia, as revealed by the summer mean surface salinity field computed from the National Oceanographic Data Center (NODC) historical data (Fig. 9**d**). The observed salinities are close to mean historical values in the region.

West of about 8.7°W longitude, an accompanying surface temperature front of 1°C divided cooler northern waters to the north from those to the south. The salinity front was partly density-compensated by the temperature. A temperature minimum extended just north of the salinity front from the northwest corner of the study region around CSV and along the continental shelf edge. This was indicative of the tongue of cool, upwelled water separated from the coast further north during the pre-cruise event. The band of warmer water along the south coast was likely continuous with the relative temperature

maximum off the west coast, just north of CSV, at about 37.1°N, but observations were too sparse to be conclusive.

3.2 Subsurface structure

Zonal CTD and ADCP sections 4 and 5 were made between 14 and 15 June west of CSV (Fig. 10) under weak southward wind stress. Stratified upper layers, with a northward intensification and shoaling of the pycnocline, accompanied southward flow in mid-section. This flow, previously observed near-surface (Fig. 5**b**), extended down to 500 m in both sections.

The southward flow in transect 5 (Fig. 10, **top**) was found between 9.4° and 9.8° W, with its core between 75 and 300 meters depth. Maximum velocities were over 0.25 ms^{-1}. The same flow in transect 4 (Fig. 10, **bottom**) lay closer to the coast, was broader, and less intense. The highest velocities (>0.20 ms^{-1}) occurred at the surface and the flow again extended down to the limit of observations. In both transects the jet-like flow coincided with the offshore side of an anomalous region of reduced vertical temperature and salinity gradient. The anomaly, clearer in transect 4 than transect 5, extended vertically from 50 m to the warm, saline MW vein at 450 m.

On the inshore side of the jet, northward flow at 0.10-0.15 ms^{-1} suggested cyclonic rotation. The temperature-salinity feature in transect 5 was compensated in the density field, which appeared quite uniform zonally over much of the transects, consistent with the largely barotropic flow. Transect 4 did show, however, a pronounced depression of the isopycnals below 100 meters depth around stations 607 and 608, associated with the more baroclinic flow there. To the east, the uplifted isotherms and isohalines broached the sea surface between stations 603 and 605 to form the density compensated surface front noted earlier. This was not seen in transect 5, which lay to the north of the front. Over the continental slope, the downward tilt of the isopycnals below 200 m depth, less evident in transect 5, was characteristic of the poleward undercurrent.

Figure 10: Vertical fields of (**a**) temperature, (**b**) salinity, (**c**) meridional velocity, and (**d**) density (σ_t) for the more northern transect 5 (**top**) and the more southern transect 4 (**bottom**) (location maps inset). Positive velocities (grey) are northward. CTD stations positions are indicated.

Figure 11: Vertical fields of (**a**) temperature, (**b**) salinity, (**c**) meridional velocity, and (**d**) density (σ_t) for transect 6 (location map inset). Positive velocities (grey) are northward. CTD stations positions are indicated.

The fine scale zonal transects made between transects 4 and 5 north of CSV, still with weak wind, showed the coastal poleward counterflow was surface intensified close to CSV. It decreased rapidly with depth from $>0.40\,\mathrm{ms}^{-1}$ near surface in transect 4 (37.08°N) (Fig. 10, **bottom**), consistent with the shoreward deepening of the isopycnals. Further north, on transect 6 (37.33°N), the vertical structure was slightly weaker with northward velocity of $>0.30\,\mathrm{ms}^{-1}$ over the inner shelf and less vertical decrease (Fig. 11). A similar pattern was found on the northernmost transect 5 (37.58°N)(Fig. 10, **top**). The near-surface poleward velocity decreased northward, while it increased in offshore extent. This flow was associated with the near-shore presence of warmer water in a region of vertically homogeneous salinity. Near geostrophic balance over the upper slope was indicated by the significant overall shoreward drop of the isopycnals.

Off the south coast, close to CSV, a similar pattern was observed. Although the flow field was not directly sampled due to a malfunction of the ADCP at the beginning of the campaign, the hydrographic fields were sampled along the meridional transect 1 (8.87°W) on 11-12 June, during the relaxation period (Fig. 12). Offshore, the fields indicated relatively uniform stratification. However, over the continental shelf edge, isotherms and isopycnals domed strongly. Thus, cooler, denser surface water was located over the shelf edge and warmer water inshore, as had been seen north of CSV in transects 4-6 (Fig. 10 and Fig. 11). Close to shore the salinity was lower and vertically uniform, but offshore of the temperature front, the isohalines intersected the surface, rising from as deep as 200 meters to form a strong surface salinity front. Again, this pattern was similar to that north of CSV, suggesting a continuity of the near-shore water mass around the cape. The

Figure 12: Vertical fields of (**a**) temperature, (**b**) salinity, and (**c**) density (σ_t) for transect 1 (location map inset). CTD stations positions are indicated.

Figure 13: Vertical fields of (**a**) temperature, (**b**) salinity, (**c**) zonal velocity, and (**d**) density (σ_t) for transect 9 (location map inset). Positive velocities (grey) are eastward. CTD stations positions are indicated.

short transect 9 (8.77°W) (Fig. 13), made about 6 days later slightly east of transect 1, showed a similar pattern. Despite the time interval between the transects, the persistence of weak wind allowed the structure of the coastal waters to remain essentially unchanged. The isolines domed over the shelf edge more weakly than before, due to a surface warming of 1-2°C relative to transect 1 and a weak salinity stratification on the shelf. Lighter and warmer water lay near shore, where shallow westward flow coincided with the drop of isotherms and isopycnals. Westward flow was also trapped over the slope with a core at about 200 m depth. The MW vein was detectable close to the continental slope at depths below 450 meters in both transects.

A dramatic change in the wind forcing occurred after 19 of June (Fig. 2 and Fig. 3). Transect 13 (8.30°W) (Fig. 14), the easternmost transect off the south coast, was carried out under northeasterly to easterly winds with speeds about $10\,\mathrm{ms}^{-1}$. However, a period of about 17 hours of intense wind with a strong westerly component ($\approx 12\,\mathrm{ms}^{-1}$) occurred just before the sampling (Fig. 3). Thus, the near-surface isopycnals were relatively horizontal in contrast to earlier meridional transects 1 and 9. As expected from Ekman transport and geostrophic adjustment, the alongshore flow was eastward in the upper layers. This flow was centred at about 36.75°N and weakened towards the coast, although no coastal counterflow was observed. The continuous tilt of the 14°C and shallower isotherms up the slope from more than 200 meters depth is indicative of strong upwelling. The isohalines rose from similar depths to form a surface salinity front, as in transect 9 (Fig. 13). Below the eastward flow (>300 m depth) and further offshore, the flow was weakly westward. The shallow vein of MW was constrained to the slope below 400 meters.

Figure 14: Vertical fields of (**a**) temperature, (**b**) salinity, (**c**) zonal velocity, and (**d**) density (σ_t) for transect 13 (location map inset). Positive velocities (grey) are eastward. CTD stations positions are indicated.

4 Discussion and Summary

The study took place just after the cessation of an upwelling episode, when winds had weakened and no upwelling was present. Analysis of thermal infrared AVHRR imagery and hydrographic and velocity data in the CSV region revealed the presence of interleaved opposing flows, reflecting the interaction of two regimes summarized in the conceptual model of Fig. 15.

One was upwelling forced and represented by the southward, cold, low salinity, jet-like flow off the west coast, which turned eastward around CSV along the continental shelf break and slope. Its offshore boundary was associated with a strong salinity front and weaker, irregular density front. It seemed to arise from the upwelling and equatorward flow along the west coast prior to the cruise. With weak winds during the cruise, this flow appeared to lose momentum while turning eastward along the south coast. More energetic and persistent equatorward winds might have caused the flow to form a cold filament south of CSV.

The other regime consisted of a narrow inshore warm counterflow that developed along the south coast. The flow was continuous from the Gulf of Cadiz in the east, curled anticyclonically around CSV with velocities up to $0.40\,\mathrm{ms}^{-1}$, and progressed poleward to over 37.5°N in the absence of opposing equatorward wind. The horizontal shears between counterflow and southward jet resulted in smaller scale instabilities seen as cyclonic eddies on the inshore flank of the jet. Anticyclonic eddies of similar size developed on its offshore boundary. The transfer of kinetic energy of rotation from the main flow to the perturbations implies a decay of the flow in the absence of upwelling-favourable winds as it proceeds south and around the Cape. Near the end of the study, re-establishment of westerly winds on the south coast produced an upwelling event and eastward flow against

the alongshore pressure gradient. Superimposed on these patterns, inertial currents were excited in the upper layers by the wind pulse.

Somewhat similar inshore poleward counter-currents have been observed to recur during the upwelling season off California, whenever upwelling favourable winds relax (Huyer and Kosro, 1987; Send et al., 1987; Winant et al., 1987). Alongshore pressure gradients have been acknowledged as a major forcing for the poleward flow on the inner shelf. Mechanisms proposed for their set up include wind stress curl (Wang, 1997), interaction of wind-driven currents with shelf topography (Jianping and Allen, 2002), and alongshore variation of upwelling (Harms and Winant, 1998; Winant et al., 2003). The appearances of coastal surface counter-currents were always associated with particular spatially limited features such as capes, rather than forming any continuous pattern along the coast.

The dynamical forcing of the inshore countercurrent near CSV is also attributed to the interplay between a regional alongshore pressure gradient and the wind forcing (Relvas and Barton, 2002). Any effect of the wind directly driving the development of the inshore warm circulation can be dismissed because of the lack of poleward wind at any time during the survey. Relvas and Barton (2002) concluded that the driving factor of the alongshore pressure gradient was present during most of the year but enhanced during the summer months. Although the investigation of the driving mechanisms of the inshore warm countercurrent is beyond the scope of the present study, it seems probable that the alongshore currents in the CSV coastal region are closely linked to forcing in the Gulf of Cádiz. For instance, it can be hypothesised that the mechanism proposed by Mauritzen et al. (2001) of excess Atlantic Water entering the Gulf of Cádiz from the Azores Current produces the alongshore pressure gradient.

The situation here is particularly similar to that of the Southern California Bight (Winant et al., 2003), where the coastal configuration around Point Conception resembles that near CSV, but there are significant differences between the two zones. South of Point Conception, the Santa Barbara Channel is bounded by the Channel Islands to form a restricted entrance to the Southern California Bight. The relatively shallow channel

plays an important role in forming re-circulation patterns (Harms and Winant, 1998), in contrast to CSV, where communication with the Gulf of Cadiz is unimpeded over deep ocean. Nevertheless, the competition between wind stress and alongshore pressure gradient forcing seems similar in the two areas. In both cases, wind sheltering equatorward of the cape results in weaker upwelling than on the exposed west coast and permits the effect of the alongshore pressure gradient to be seen. Also, the variability of near-shore velocity and temperature in the Southern California Bight has been ascribed to remotely forced alongshore pressure gradient disturbances propagating along the coast (Hickey et al., 2003).

The separation of the jet from the coast at Cape da Roca was observed only by remote sensing in this study. An analogous case is perhaps that studied in detail off Cape Blanco, Oregon (Barth et al., 2000), where significant re-circulation of the sub-surface poleward current was found to occur near the separation. Further *in situ* measurements are required in the Iberian area to allow detailed study of such phenomena. The separation of the jet and related development of the upwelling filament off CSV which occurs at times of persistent upwelling has never been directly observed.

The results presented here reveal the importance of remote factors in controlling the local dynamics in upwelling regions. The classical view that in these regions favourable winds force near-surface offshore transport and coherent flow along the coast, does not apply throughout the upwelling season or in all areas. During interleaving periods of wind weakening, the kinematics of these regions can be dominated by narrow counter-currents driven by remote factors. Where wind forcing is weak, as in the case of CSV region, such periods represent a significant part of the upwelling season (Relvas and Barton, 2002). The relevance of the inshore countercurrent, which advects warm water rapidly along the coast, to the spread of contaminants introduced at or near the coast, to the dispersion and retention of fish eggs and larvae, to the use of beach and shore amenities, and to the onset of Harmful Algal Blooms makes it important for detailed study.

Figure 15: Circulation scheme observed during upwelling relaxation off Cape São Vicente. Note the separated jet of cool waters upwelled further north (**J**), and its decay through the interaction with the surrounding waters (anticyclonic rotation in the offshore side (**A2**) and cyclonic in the inshore (**C1** and **C2**)). The jet curled cyclonically off the south coast (**C3**) interacting with the coastal warm counterflow (**CC**) which itself turned anticyclonically around the Cape (**A1**), inshore of upwelling remnants off Cape Sines (**U**). The possible signature of a deeper meddy is labelled (**M**).

Acknowledgements. Authors would like to thank to Lúcilia Coelho and Uwe Piaktowski for facilitating our participation in the POSEIDON 201/9 cruise. Thanks are due to Peter Baylis and staff at the Dundee Satellite Receiving Station, Dundee University and to Steve Groom and Peter Miller, from the NERC Remote Sensing Data Analysis Service, CCMS-PLM, Plymouth for help with the satellite data and image processing. We thank MARETEC, Instituto Superior Técnico, Lisboa for running the tidal model for the Cape São Vicente region. This work was partially funded by Fundação para a Ciência e Tecnologia grants Ciência BD/1532/91-IG and PRAXIS XXI BD/4079/94. We thank Curt Storlazzi for a helpful review of the paper.

References

Ambar, I., 1983. A shallow core of Mediterranean water off western Portugal, *Deep Sea Res.,* 30(6A), 677-680.

Ambar, I., and M. R. Howe, 1979. Observations of the Mediterranean outflow — 1. Mixing in the Mediterranean outflow, *Deep Sea Res.,* 26, 535-554.

Barth, J. A., and K. H. Brink, 1987. Shipboard acoustic doppler profiler velocity observations near Point Conception: Spring 1983, *J. Geophys. Res.,* 92(C4), 3925-3943.

Barth, J. A., S. D. Pierce, and R. L. Smith, 2000. A separating coastal upwelling jet at Cape Blanco, Oregon and its connection to the California Current System, *Deep Sea Res. II,* 47, 783-810.

Bower, A. S., L. Armi, and I. Ambar, 1997. Lagrangean observations of Meddy formation during A Mediterranean Undercurrent Seeding Experiment, *J. Phys. Oceanogr.,* 27, 2545-2575.

Fanjul, E. A., B. P. Gómez, and I. R. Sánchez-Arévalo, 1997. A description of the tides in the Eastern North Atlantic, *Prog. Oceanogr.,* 40, 217-244.

Firing, E. and J. Ranada, 1995. Access to the CODAS High-Resolution Shipboard ADCP Data Sets. Manual version 3.1 from the Joint Institute for Marine and Atmospheric Research. School of Ocean and Earth Science and Technology, University of Hawaii, 124 pp.

Fiúza, A. F. G., 1982. The Portuguese coastal upwelling system, in *Actual Problems of Oceanography in Portugal.* pp. 45-71, Junta Nacional de Investigação Científica e Tecnológica, Lisbon.

Fiúza, A. F. G., 1983. Upwelling patterns off Portugal, in *Coastal Upwelling: Its Sediment Record*, part A, edited by E. Suess and J. Thiede, pp. 85-98, Plenum, New York.

Fiúza, A. F. G., M. E. Macedo, and M. R. Guerreiro, 1982. Climatological space and time variation of the portuguese coastal upwelling, *Oceanol. Acta,* 5, 31-40.

Frouin, R., A. F. G. Fiúza, I. Ambar, and T. J. Boyd, 1990. Observations of a poleward surface current off the coasts of Portugal and Spain during winter, *J. Geophys. Res.,* 95(C1), 679-691.

Harms, S., and C. D. Winant, 1998. Characteristic patterns of the circulation in the Santa Barbara Channel, *J. Geophys. Res.,* 103(C2), 3041-3065.

Haynes, R., and E. D. Barton, 1990. A poleward flow along the Atlantic coast of the Iberian Peninsula, *J. Geophys. Res.,* 95(C7), 11,425-11,442.

Hickey, B. M., E. L. Dobbins, and S. E. Allen, 2003. Local and remote forcing of currents and temperature in the central Southern California Bight, *J. Geophys. Res.,* 108(C3), 3081, doi:10.1029/2000JC000313.

Hinrichsen, H.-H., M. Rein, R. H. Käse, and W. Zenk, 1993. The Mediterranean water tongue and its chlorofluoromethane signal in the Iberian basin in early summer 1989, *J. Geophys. Res.,* 98(C5), 8405-8412.

Huthnance, J. M., Slope currents and JEBAR, 1984. *J. Phys. Oceanogr.,* 14, 795-810.

Huyer, A., and P. M. Kosro, 1987. Mesoscale surveys over the shelf and slope in the upwelling region near Point Arena, California, *J. Geophys. Res.,* 92(C2), 1655-1681.

Huyer, A., P. M. Kosro, J. Fleischbein, S. Ramp, T. Stanton, L. Washburn, F. P. Chavez, T. J. Cowles, S. D. Pierce, and R. L. Smith, 1991. Currents and water masses of the coastal transition zone off northern California, June to August 1988, *J. Geophys. Res.,* 96(C8), 14,809-14,831.

Jianping, G., and J. S. Allen, 2002. A modeling study of shelf circulation off northern California in the region of the Coastal Ocean Dynamics Experiment: Response to relaxation of upwelling winds, *J. Geophys. Res.,* 107(C9), 3123, doi:10.1029/2000JC000768.

Large, W., and S. Pond, 1981. Open Ocean momentum flux measurements in moderate to strong winds, *J. Phys. Oceanogr.,* 11, 324-336.

Mauritzen C., Y. Morel, and J. Paillet, 2001. On the influence of Mediterranean Water on the Central Waters of the North Atlantic Ocean, *Deep Sea Res.,* 48, 347-381.

McClain, E. P., W. G. Pichel, and C. C. Walton, 1985. Comparative perfomance of AVHRR-based multichannel sea surface temperatures, *J. Geophys. Res.,* 90, 11587-11601.

Meincke, J., G. Siedler, and W. Zenk, 1975. Some current observations near the continental slope off Portugal, *Meteor Forschungsergebnisse A,* 16, 15-22.

Oliveira, P. B., N. Serra, A. F. G. Fiúza, and I. Ambar, 2000. A study of meddies using simultaneous in-situ and satellite observations, In *Satellites, Oceanography and Society*, edited by D. Halpern, Elsevier Science B. V., 125-148.

Pollard, R. T., and S. Pu, 1985. Structure and circulation of the upper Atlantic ocean northeast of the Azores, *Prog. Oceanogr.,* 14, 443-462.

Pollard, R. and J. Read, 1989. A method for calibrating shipmounted Acoustic Doppler Current Profilers, and the limitations of gyro-compasses, *J. Atmos. Oceanic Technol.*,6, 859-865.

Prater, M. D., and T. B. Sanford, 1994. A Meddy off Cape St. Vincent. Part I: Description, *J. Phys. Oceanogr.,* 24, 1572-1586.

Ramp, S. R., P. F. Jessen, K. H. Brink, P. P. Niiler, F. L. Daggett, and J. S. Best, 1991. The physical structure of cold filaments near Point Arena, California, during June 1987, *J. Geophys. Res.,* 96(C8), 14,859-14,883.

Reid, J. L., and A. W. Mantyla, 1976. The effect of the geostrophic flow upon elevations in the northern North Pacific ocean, *J. Geophys. Res.,* 81(18), 3100-3110.

Relvas, P. and E.D. Barton, 1995. Poseidon Cruise 201/9 Report: Physical Oceanography Data Report, 284pp., University of Algarve, Faro.

Relvas, P. and E.D. Barton, 1996. Poseidon Cruise 201/9 Report: Acoustic Doppler Current Profiler Data – Velocity Fields, 51pp., University of Algarve, Faro.

Relvas, P. and E.D. Barton, 2002. Mesoscale patterns in the Cape São Vicente (Iberian Peninsula) upwelling region, *J. Geophys. Res.,* 107(C10), 3164, doi:10.1029/2000JC000456.

Rhein, M., and H.-H. Hinrichsen, 1993. Modification of Mediterranean water in the Gulf of Cadiz, studied with hydrographic and chlorofluoromethanes data, *Deep Sea Res.,* 40, 267-291.

Send, U., R. C. Beardsley, and C. D. Winant, 1987. Relaxation from upwelling in the coastal ocean dynamics experiment, *J. Geophys. Res.,* 92(C2), 1683-1698.

Serra, N., S. Sadoux, I. Ambar, and D. Renouard, 2002. Observations and laboratory modeling of Meddy generation at Cape St. Vincent, *J. Phys. Oceanogr.,* 32, 3-25.

Stammer, D., H. H. Hinrichsen, and R. H. Käse, 1991. Can meddies be detected by satellite altimetry?, *J. Geophys. Res.,* 96(C4), 7005-7014.

Trenberth, K. E., W. G. Large and J. G. Olson, 1990. The mean annual cycle in global ocean wind stress, *J. Phys. Oceanogr.,* 20, 1742-1760.

Tychensky, A., and X. Carton, 1998. Hydrological and dynamical characterization of meddies in the Azores region: A paradigm for baroclinic vortex dynamics, *J. Geophys. Res.,* (C11), 25.061-25.079.

UNESCO, *Technical Papers in Marine Science,* JPOTS panel, Processing of Oceanographic Station Data, 138 pp., Paris, 1991.

Wang, D-P., 1997. Effects of small-scale wind on coastal upwelling with application to Point Conception, *J. Geophys. Res.,* 102(C7), 15555-15566.

Winant, C. D., R. C. Beardsley, and R. E. Davis, 1987. Moored wind, temperature and current observations made during Coastal Ocean Dynmics Experiment 1 and 2 over the northern California continental shelf and upper slope, *J. Geophys. Res.,* 92, 1569-1604.

Winant, C. D., E. P. Dever, and M. C. Hendershott, 2003. Characteristic patterns of shelf circulation at the boundary between central and southern California, *J. Geophys. Res.,* 108(C2), 3021, doi:10.1029/2001JC001302.

Wooster, W. S., A. Bakun, and D. R. McLain, 1976. The seasonal upwelling cycle along the eastern boundary of the North Atlantic, *J. Mar. Res.,* 34, 131-141.

Zenk, W., 1975. On the Mediterranean outflow west of Gibraltar, *Meteor Forschungsergebnisse A,* 16, 23-34.

Zenk, W., and L. Armi, 1990. The complex spreading pattern of Mediterranean Water off the Portuguese continental slope, *Deep Sea Res.,* 37(12), 1805-1823.

List of Figures

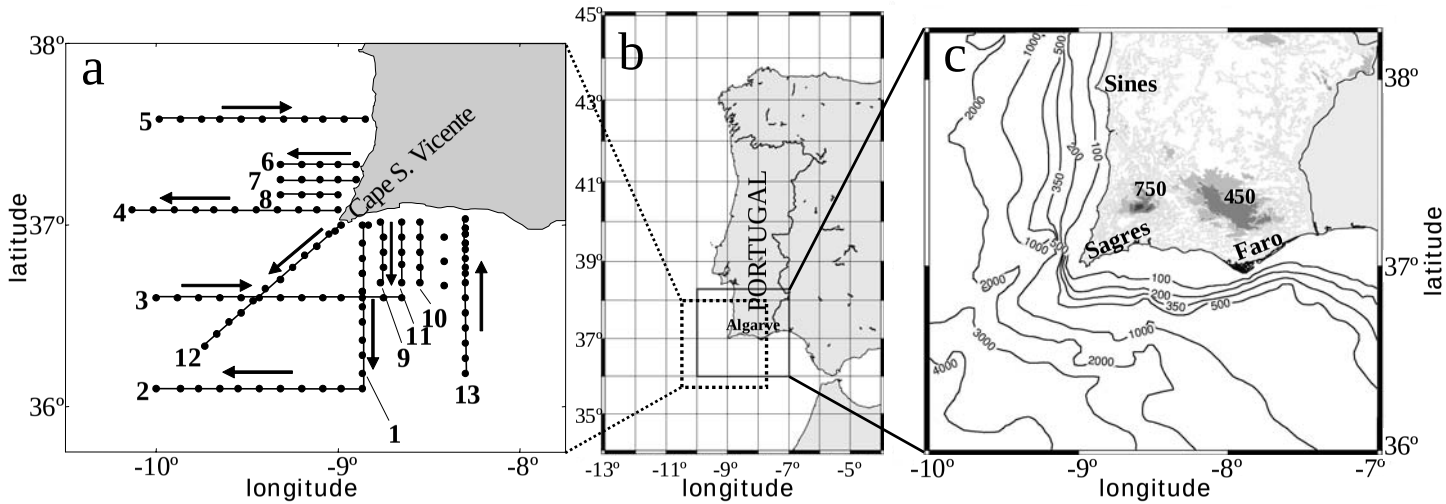
a
b
c
Cape S. Vicente
PORTUGAL
Algarve
Sines
Sagres
Faro
750
450
latitude
longitude
38º
37º
36º
-10º
-9º
-8º
45º
43º
41º
39º
37º
35º
-13º
-11º
-9º
-7º
-5º
-7º
1
2
3
4
5
6
7
8
9
10
11
12
13

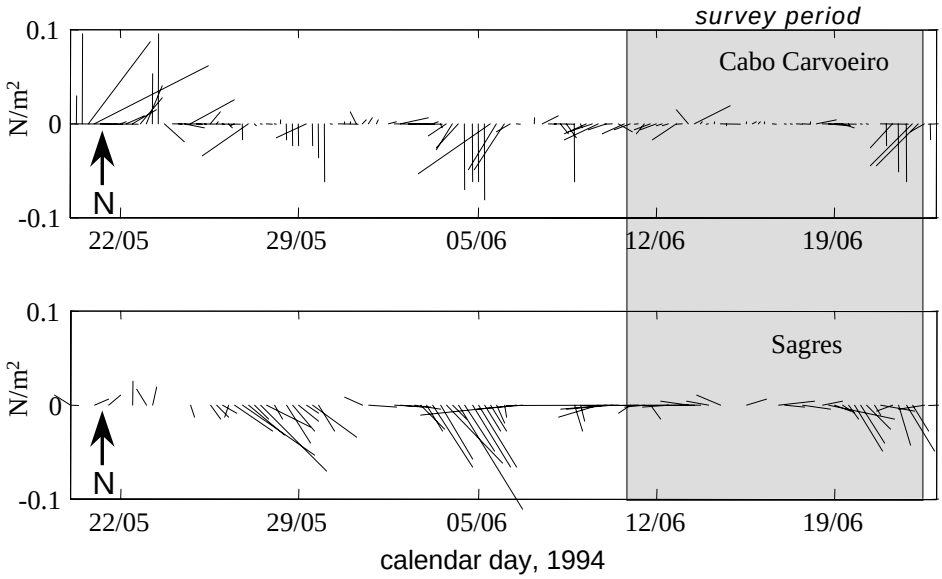
survey period
Cabo Carvoeiro
Sagres
0.1
0
-0.1
N/m2
N
22/05
29/05
05/06
12/06
19/06
calendar day, 1994

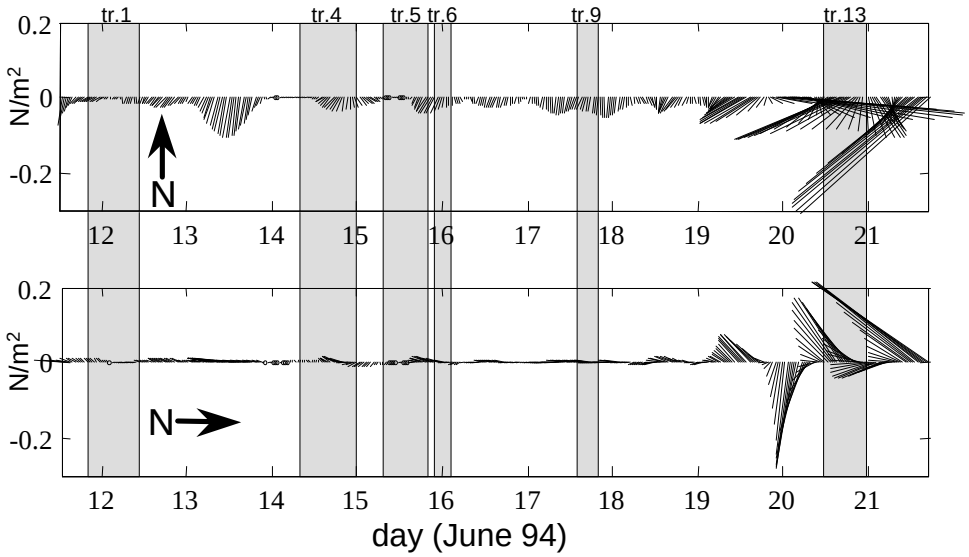
tr.1
tr.4
tr.5
tr.6
tr.9
tr.13
0.2
0
-0.2
N/m2
N
12
13
14
15
16
17
18
19
20
21
0.2
0
-0.2
N/m2
N
12
13
14
15
16
17
18
19
20
21
day (June 94)

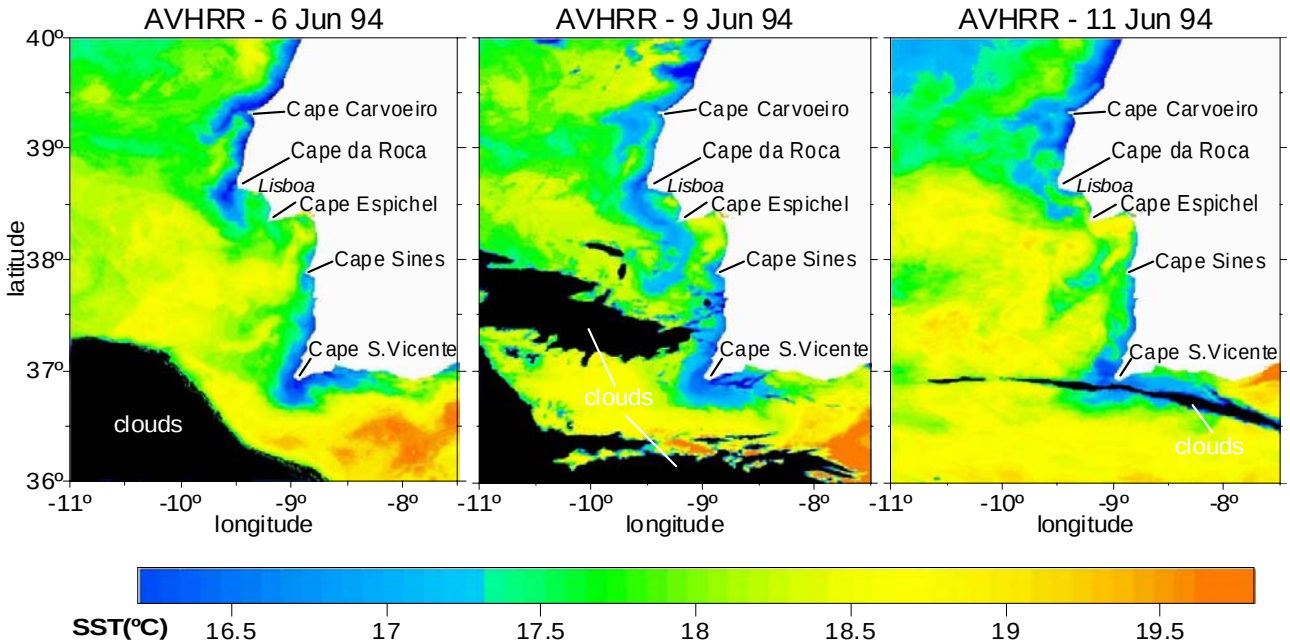
AVHRR - 6 Jun 94
AVHRR - 9 Jun 94
AVHRR - 11 Jun 94
Cape Carvoeiro
Cape da Roca
Lisboa
Cape Espichel
Cape Sines
Cape S.Vicente
clouds
latitude
longitude
40º
39º
38º
37º
36º
-11º
-10º
-9º
-8º
SST(ºC)
16.5
17
17.5
18
18.5
19
19.5

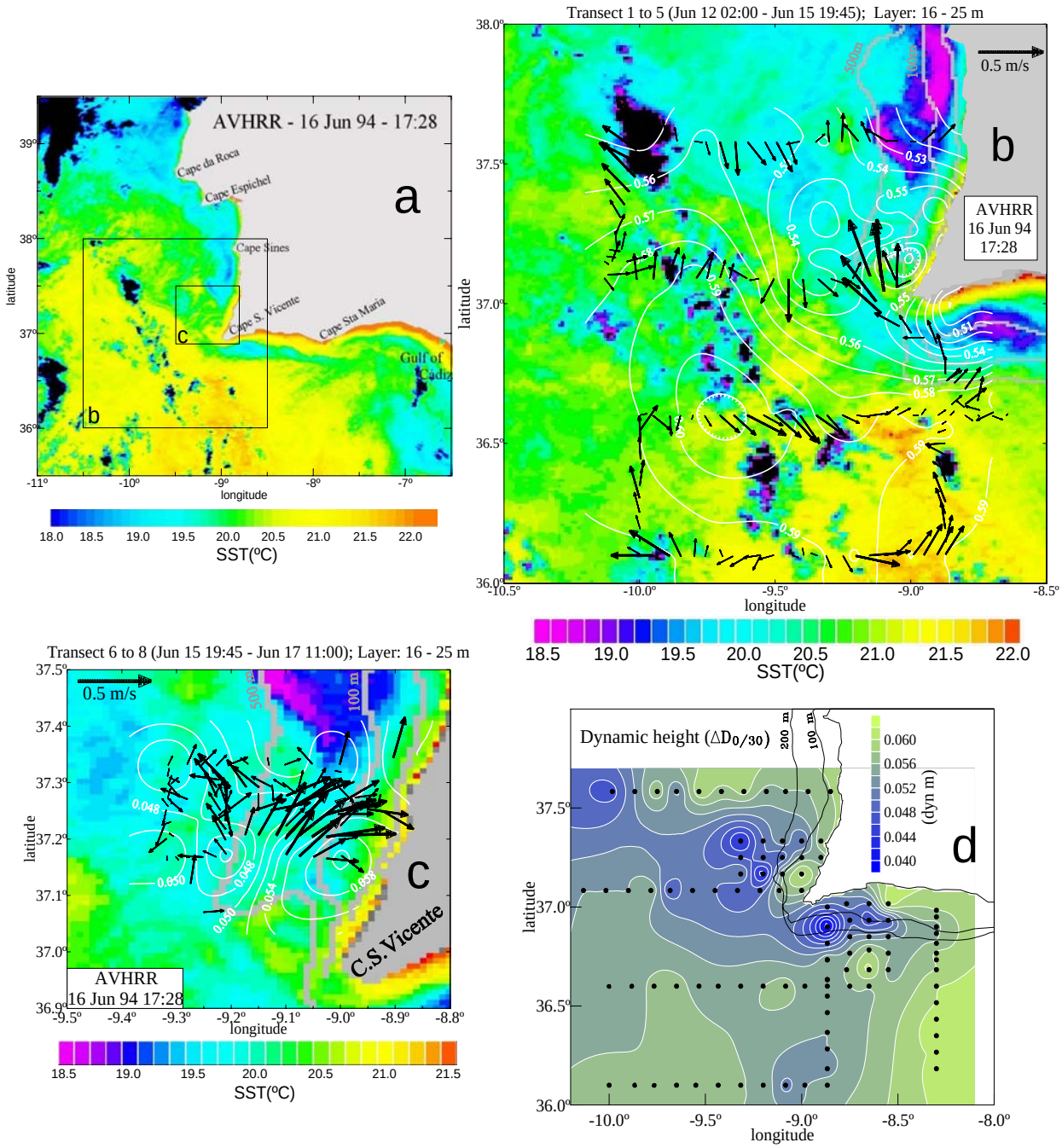
AVHRR - 16 Jun 94 - 17:28
a
Cape da Roca
Cape Espichel
Cape Sines
Cape S. Vicente
Cape Sta Maria
Gulf of Cadiz
b
c
latitude
longitude
SST(ºC)
Transect 1 to 5 (Jun 12 02:00 - Jun 15 19:45); Layer: 16 - 25 m
0.5 m/s
AVHRR
16 Jun 94
17:28
Transect 6 to 8 (Jun 15 19:45 - Jun 17 11:00); Layer: 16 - 25 m
C.S. Vicente
Dynamic height (ΔD0/30)
(dyn m)

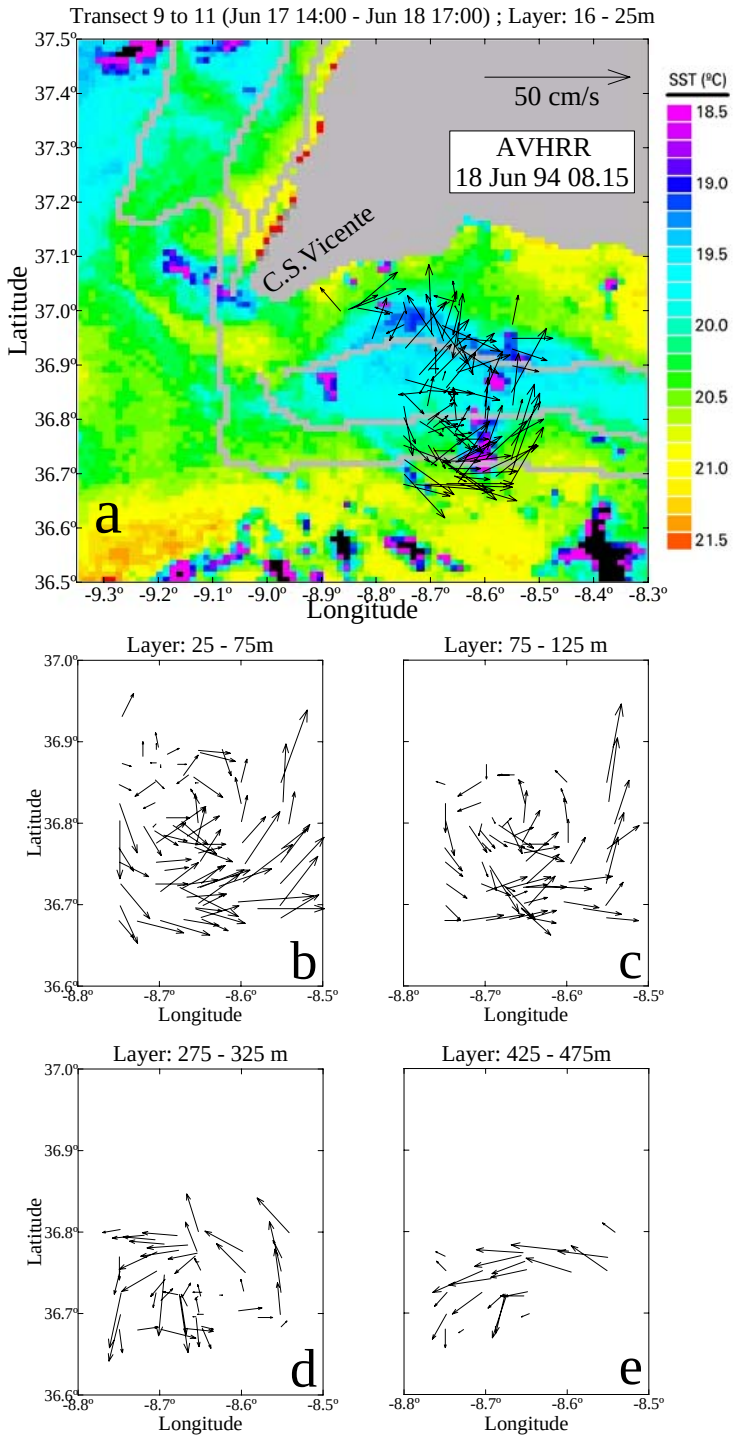
Transect 9 to 11 (Jun 17 14:00 - Jun 18 17:00) ; Layer: 16 - 25m
50 cm/s
AVHRR
18 Jun 94 08.15
C.S.Vicente
SST (ºC)
18.5
19.0
19.5
20.0
20.5
21.0
21.5
Latitude
Longitude
a
Layer: 25 - 75m
Layer: 75 - 125 m
Layer: 275 - 325 m
Layer: 425 - 475m
b
c
d
e

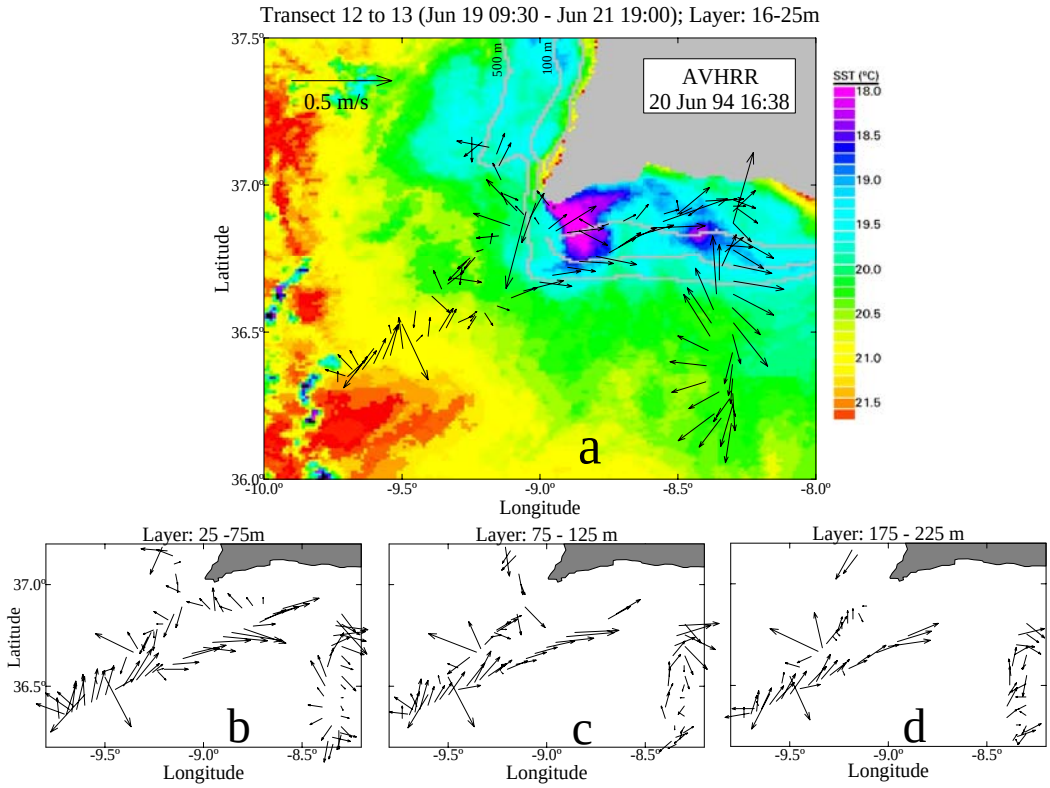
Transect 12 to 13 (Jun 19 09:30 - Jun 21 19:00); Layer: 16-25m
0.5 m/s
500 m
100 m
AVHRR
20 Jun 94 16:38
SST (ºC)
18.0
18.5
19.0
19.5
20.0
20.5
21.0
21.5
a
Latitude
Longitude
37.5º
37.0º
36.5º
36.0º
-10.0º
-9.5º
-9.0º
-8.5º
-8.0º
Layer: 25 -75m
Layer: 75 - 125 m
Layer: 175 - 225 m
b
c
d

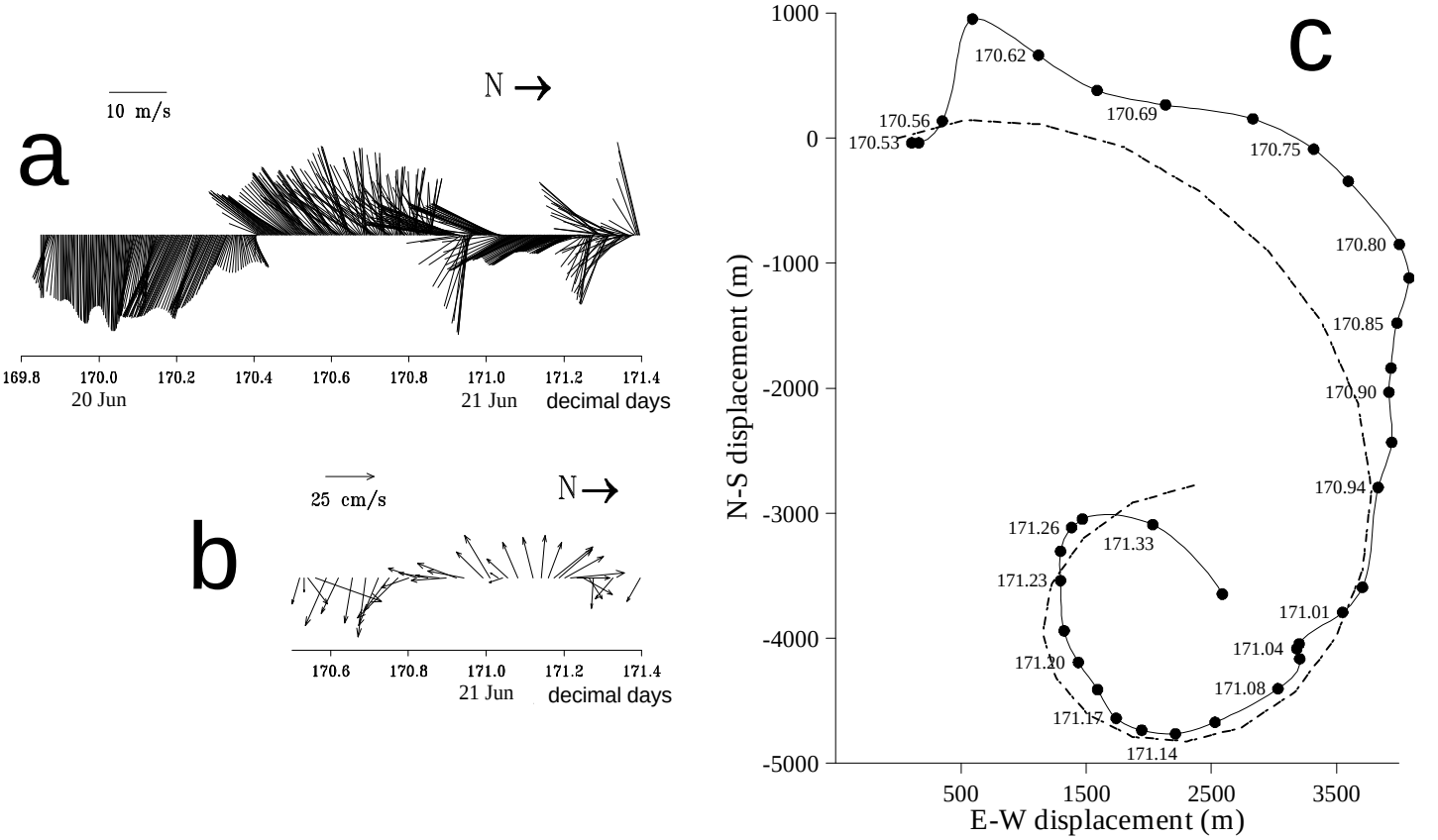
a
10 m/s
N →
169.8
170.0
170.2
170.4
170.6
170.8
171.0
171.2
171.4
20 Jun
21 Jun
decimal days
b
25 cm/s
N →
170.6
170.8
171.0
171.2
171.4
21 Jun
decimal days
c
N-S displacement (m)
E-W displacement (m)
1000
0
-1000
-2000
-3000
-4000
-5000
500
1500
2500
3500
170.53
170.56
170.62
170.69
170.75
170.80
170.85
170.90
170.94
171.01
171.04
171.08
171.14
171.17
171.20
171.23
171.26
171.33

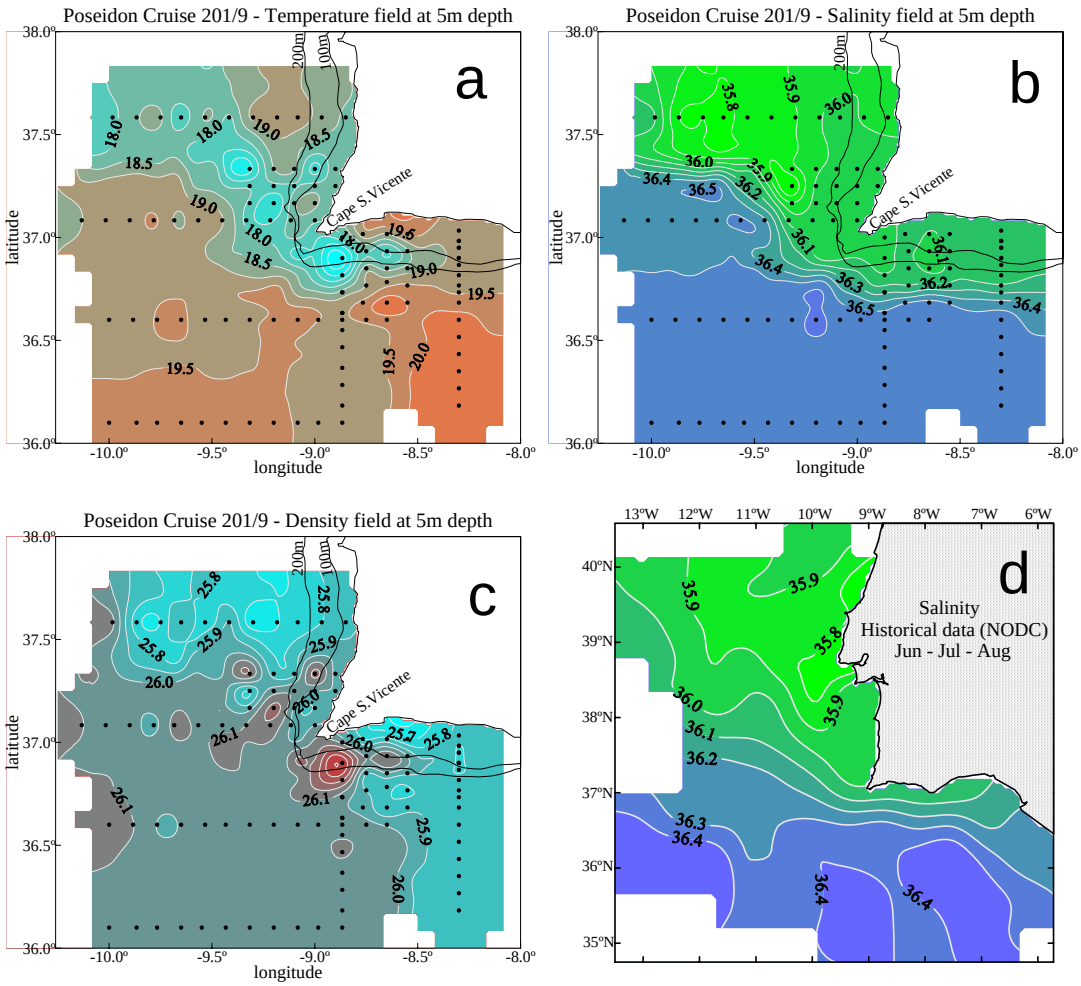
Poseidon Cruise 201/9 - Temperature field at 5m depth
a
Cape S.Vicente
200m
100m
latitude
longitude
Poseidon Cruise 201/9 - Salinity field at 5m depth
b
Cape S.Vicente
Poseidon Cruise 201/9 - Density field at 5m depth
c
Cape S.Vicente
d
Salinity
Historical data (NODC)
Jun - Jul - Aug

Transect 5 - Jun 15 08:23 - Jun 15 19:24

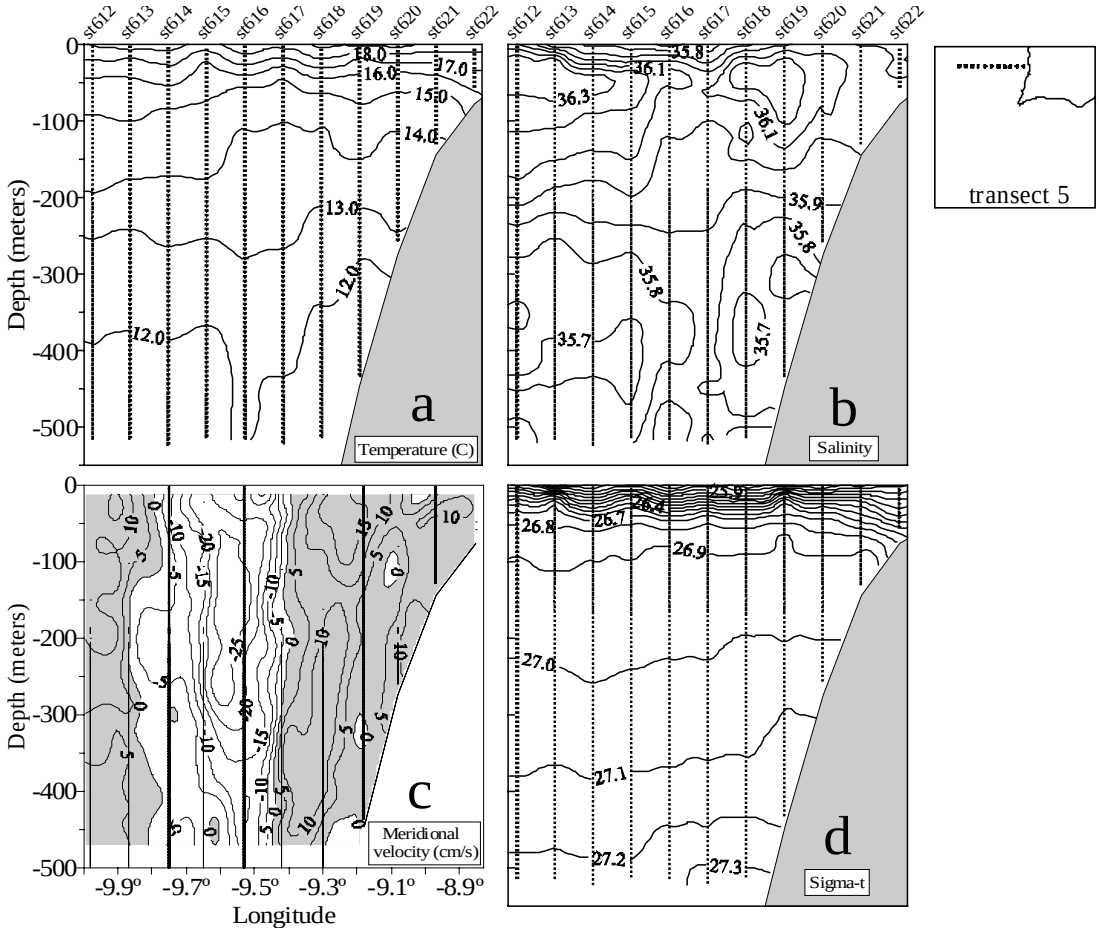

Transect 4 - Jun 14 08:59 - Jun 15 00:00

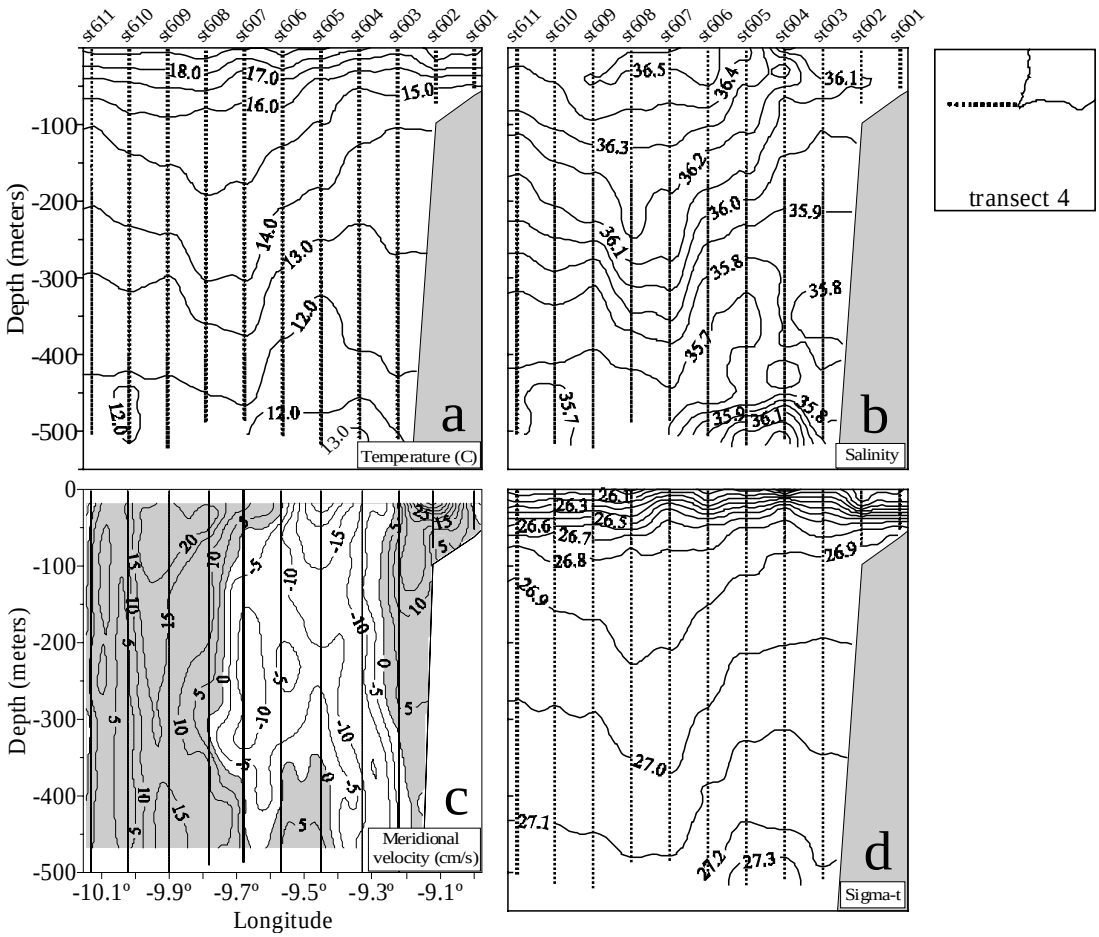

Transect 6 - Jun 15 21:44 - Jun 16 01:47

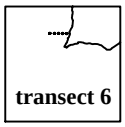

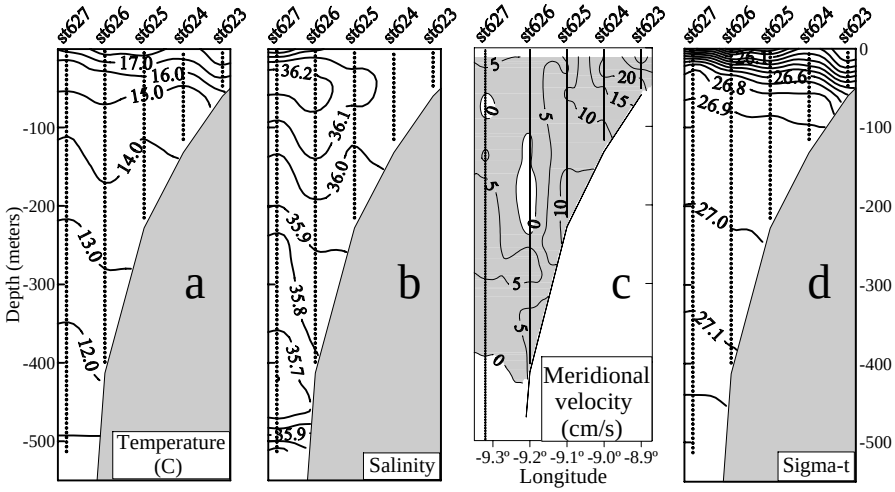

Transect 1 - Jun 11 19:34 - Jun 12 10:05

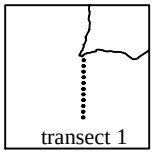

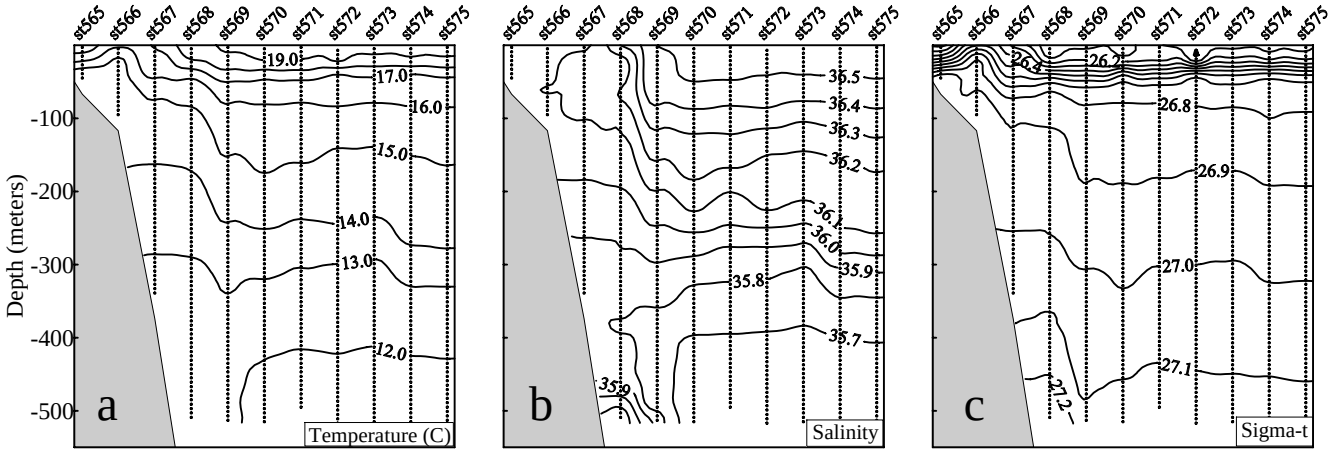

Transect 9 - Jun 17 14:53 - Jun 17 19:30

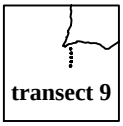

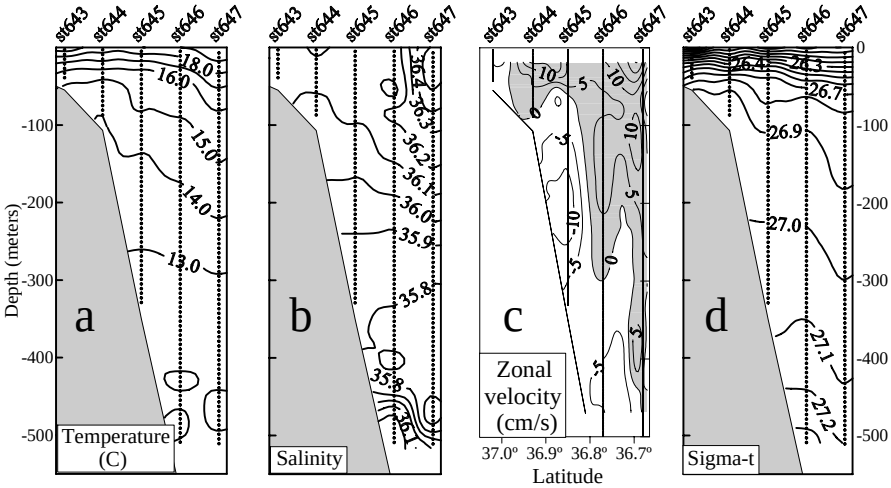

Transect 13 - Jun 20 12:14 - Jun 20 23:10

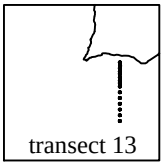

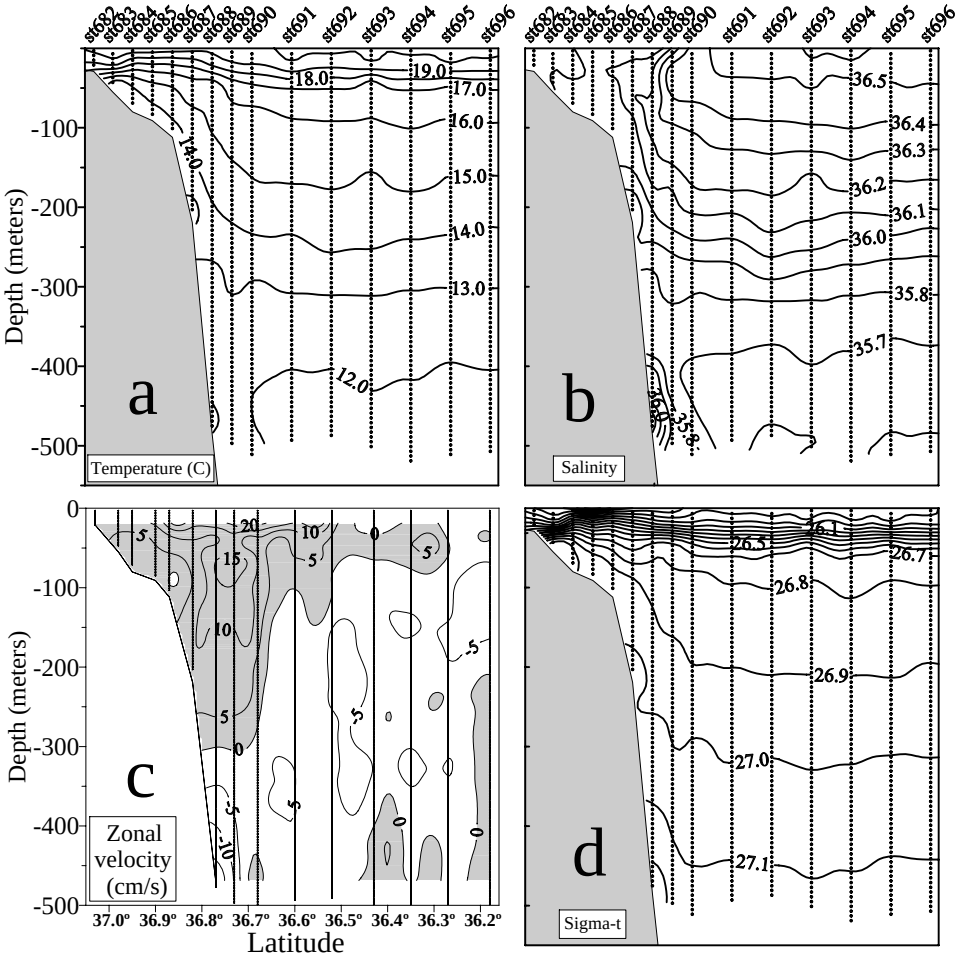

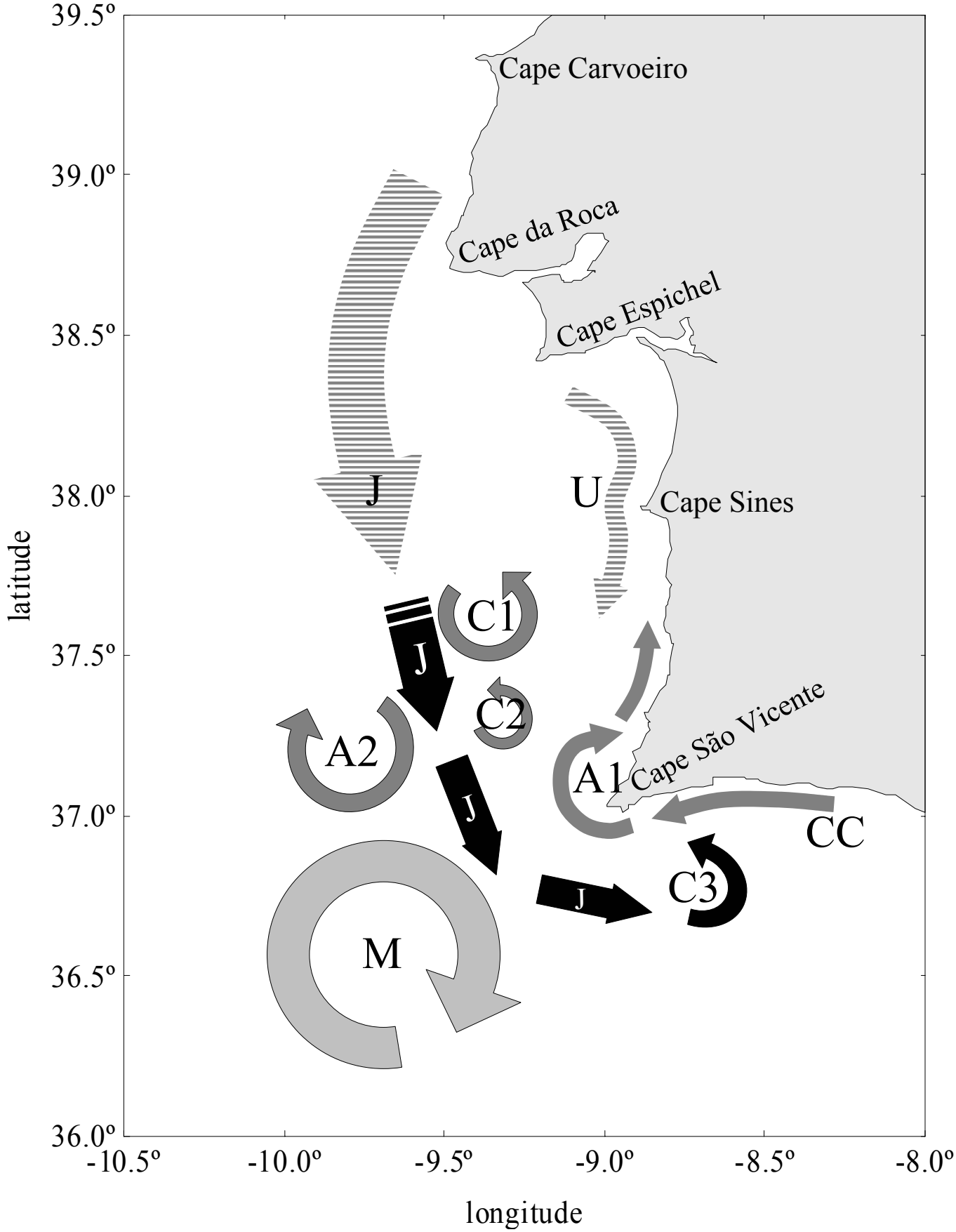
39.5º
39.0º
38.5º
38.0º
37.5º
37.0º
36.5º
36.0º
latitude
-10.5º
-10.0º
-9.5º
-9.0º
-8.5º
-8.0º
longitude
Cape Carvoeiro
Cape da Roca
Cape Espichel
Cape Sines
Cape São Vicente
J
U
C1
J
C2
A2
J
A1
CC
C3
J
M